Effects of Fiber Alignment and Coculture with Endothelial Cells on Osteogenic Differentiation of Mesenchymal Stromal Cells

TISSUE ENGINEERING: Part C
Volume 26, Number 1, 2020

DOI: 10.1089/ten.tec.2019.0232

termis
Tissue Engineering
& Regenerative Medicine
International Society

METHODS ARTICLE

Effects of Fiber Alignment and Coculture with Endothelial Cells on Osteogenic Differentiation of Mesenchymal Stromal Cells

Tianyu Yao, MSc,[1] Honglin Chen, PhD,[2] Matthew B. Baker, PhD,[1] and Lorenzo Moroni, PhD[1]

Vascularization is a critical process during bone regeneration. The lack of vascular networks leads to insufficient oxygen and nutrients supply, which compromises the survival of regenerated bone. One strategy for improving the survival and osteogenesis of tissue-engineered bone grafts involves the coculture of endothelial cells (ECs) with mesenchymal stromal cells (MSCs). Moreover, bone regeneration is especially challenging due to its unique structural properties with aligned topographical cues, with which stem cells can interact. Inspired by the aligned fibrillar nanostructures in human cancellous bone, we fabricated polycaprolactone (PCL) electrospun fibers with aligned and random morphology, cocultured human MSCs with human umbilical vein ECs (HUVECs), and finally investigated how these two factors modulate osteogenic differentiation of human MSCs (hMSCs). After optimizing cell ratio, a hMSCs/HUVECs ratio (90:10) was considered to be the best combination for osteogenic differentiation. Coculture results showed that hMSCs and HUVECs adhered to and proliferated well on both scaffolds. The aligned structure of PCL fibers strongly influenced the morphology and orientation of hMSCs and HUVECs; however, fiber alignment was observed to not affect alkaline phosphate (ALP) activity or mineralization of hMSCs compared with random scaffolds. More importantly, cocultured cells on both random and aligned scaffolds had significantly higher ALP activities than monoculture groups, which indicated that coculture with HUVECs provided a larger relative contribution to the osteogenesis of hMSCs compared with fiber alignment. Taken together, we conclude that coculture of hMSCs with ECs is an effective strategy to promote osteogenesis on electrospun scaffolds, and aligned fibers could be introduced to regenerate bone tissues with oriented topography without significant deleterious effects on hMSCs differentiation. This study shows the ability to grow oriented tissue-engineered cocultures with significant increases in osteogenesis over monoculture conditions.

Keywords: electrospun, coculture, alignment, bone regeneration, vascularization

Impact Statement

This work demonstrates an effective method of enhancing osteogenesis of mesenchymal stromal cells on electrospun scaffolds through coculturing with endothelial cells. Furthermore, we provide the optimized conditions for cocultures on electrospun fibrous scaffolds and engineered bone tissues with oriented topography on aligned fibers. This study demonstrates promising findings for growing oriented tissue-engineered cocultures with significant increase in osteogenesis over monoculture conditions.

Introduction

Bone is a highly vascularized tissue, which contains multiple cell types, including osteogenic and endothelial cells (ECs).[1,2] Blood vessels can provide oxygen, nutrition, and metal ions for osteogenic cells during bone regeneration.[3,4] Lack of efficient vascularization limits the size of new bone formation and even leads to cell death in bone graft.[5–8] Therefore, vascularization is a great challenge in bone tissue engineering.[9,10] In an attempt to solve this

[1]Complex Tissue Regeneration Department, MERLN Institute for Technology Inspired Regenerative Medicine, Maastricht University, Maastricht, The Netherlands.
[2]Institute for Life Science, School of Medicine, South China University of Technology, Guangzhou, China.

problem, coculture techniques have been widely used for vascularized bone tissue engineering.[11] Several studies have highlighted the interaction between osteogenic cells and ECs using coculture systems as tools for mimicking the communication between these cells in living tissue.[12–14] For example, the coculture of human mesenchymal stem cells (hMSCs) and human umbilical vein ECs (HUVECs) spheroid by seeding ≤2% HUVECs was used to create perivascular networks *in vitro*, and finally induced osteogenic differentiation of hMSCs.[15] The cocultured groups had higher alkaline phosphate (ALP) activity compared with monocultures, showing that ECs promoted osteogenic differentiation of hMSCs.[16,17] In another study, a cell sheet model on polyvinylidene fluoride (PVDF) membrane combining bone marrow stem cells with ECs was proven to be a useful strategy for the prevascularization of tissue regeneration. These cell sheet-based constructs improved the survival of bone implantation by promoting the formation and stabilization of vascular units.[18] Therefore, cocultures of hMSCs with ECs could be an effective strategy for vascularized bone formation.

The surface topography of biomaterials is considered to be one of the crucial parameters in determining cell activity.[19–21] In particular, the effect of surface topography on stem cell differentiation has been extensively investigated.[22–24] Previous reports indicated that different nanopatterns, mechanical properties, and geometrical cues of scaffolds showed a significant effect on regulating stem cells behavior.[25] There are several kinds of nanopatterns, which have been previously studied, such as grooves,[26,27] nanopillars,[28,29] nanopits,[30] and aligned fibers.[31,32] In the bone matrix, collagen fibers are preferentially oriented (parallel to the long axis of bone), and their structural features are important to provide strength in tension and resistance in bone bending.[33–35] Since native bone tissue is composed of highly aligned collagen fibers,[36] researchers attempted to mimic this unique structure by using aligned electrospun fibers.[31,37] The effects of fiber alignment on osteogenic differentiation have been already investigated.[38–40] It was reported that the alignment of fibers induced osteogenic differentiation and upregulated the expression of osteogenic marker genes.[31] Aligned electrospun fibers provide specific geometrical cues, which guide the structure and function of hMSCs for bone regeneration.[31,41] Calcium content on aligned fibers was significantly higher compared with that of random fibers.[38] These aligned fibrous meshes showed positive effect for bone regeneration. However, the lack of vascularization in biomaterials scaffold is still a primary challenge to support long-term functions of the regenerated bone.[42,43]

Combining the design of aligned nanofibrous scaffolds and cocultures with ECs has been considered to be a highly promising strategy for bone regeneration research.[39] Only one study reported the combination effects of these two factors on the osteogenic differentiation of hMSCs. Xu *et al.* combined structural signals of aligned electrospun scaffolds and chemical signals of bioglass ionic products, and investigated the effects of combined biomaterial signals on communications between hMSCs and HUVECs.[39] This study only showed the effect of aligned electrospun scaffolds on osteogenesis, but did not investigate if fiber alignment of the electrospun scaffolds contributed to the enhanced osteogenic differentiation. Moreover, studies on the optimization of coculture conditions on electrospun scaffolds are lacking, and more specific conditions including coculture medium and cell ratio should be taken into consideration when coculture studies are performed. Many studies reported that a coculture ratio of 1:1 (hMSCs/ECs) is the best combination to obtain osteogenic differentiation.[44,45] This ratio is also the most commonly used in the literature for coculture experiments of hMSCs/ECs.[10,46–48] Some researchers presumed that lower ratio of ECs could be beneficial for the vessels formation, and they used 98:2–98:5 for coculture studies.[1,15,49] Guided by these considerations, (1) we optimized cell ratio of hMSCs and HUVECs (98:2–50:50) on random electrospun scaffolds, and finally chose the optimal ratio on cell differentiation and mineralization for osteogenesis; (2) we developed biomimetic aligned fibrous scaffolds using a rotating mandrel as a collector, then cocultured hMSCs and HUVECs on the scaffolds. The influence of aligned topography on the behavior of cocultured HUVECs and hMSCs was studied. We hypothesized that hMSC/HUVEC cocultures may behave differently on the random and aligned fibrous scaffolds as illustrated in Figure 1. The aligned fibers may guide the structural assembly of collagen with an alignment that is closer to native bone environment for regeneration. Subsequently, we focus on an *in vitro* assessment of the osteogenic differentiation potential of hMSCs by quantifying ALP activity and calcium content in the biological constructs. We were interested in investigating the effect of two combined factors (tissue-mimetic nanotopography and coculture with ECs) on hMSCs differentiation and subsequent mineralization.

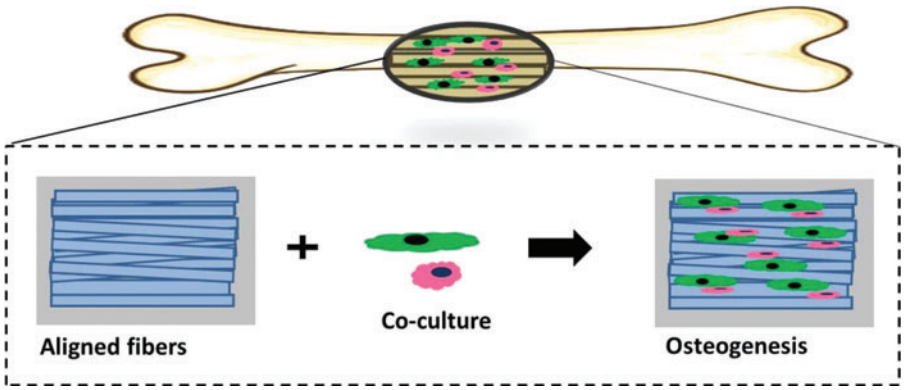

FIG. 1. Schematic illustrating the coculture of hMSCs with ECs on aligned electrospun fibers. ECs, endothelial cells; hMSCs, human mesenchymal stromal cells. Color images are available online.

Materials and Methods

Fabrication of random and different aligned fibers

Poly(caprolactone) (PCL; Mn = 70–90k) was produced by Sigma-Aldrich. PCL was dissolved in chloroform-dimethylformamide (4:1) mixture to prepare final concentrations of 15% (w/v) for random and aligned fibers. Homogeneous solutions were prepared with gentle stirring overnight. A homemade electrospinning setup applied in our study was reported before.[50] The setup is made up of a plastic syringe, a syringe pump (Harvard 2000), a stainless-steel blunt-end needle (inner diameter = 0.8 mm), an aluminum plate, and a high-voltage power supply. The random fibers were randomly deposited on the aluminum plate. For aligned fibrous mesh, a high-speed rotational mandrel was used as collector. To get high alignment, the speed of the rotating mandrel was varied from 1000 to 4600 rpm.

Characterization of random and different aligned fibers

The morphology of the random and aligned fibers was imaged by a scanning electron microscopy (SEM) (Philips XL-30 ESEM). In brief, electrospun samples were coated with gold (Cressington Sputter Coater 108 auto) for 100 s at 30 mA, and then observed by SEM at an accelerating voltage of 10 kV. All images were applied to quantitatively measure the diameter and coherency of fibers by using the Fiji software. The coherency coefficient of fibers was measured using the Orientation J plug-in of Fiji. The value of coherency usually ranges from 0 to 1; the value is close to 1 indicating a strongly coherent orientation and greater alignment.

Cell culture

hMSCs (D8011L) provided by the Institute of Regenerative Medicine (Texas A&M University, Temple, TX) were isolated from the bone marrow and proliferated as described previously.[51] Cells were first cultured in a basic medium, including α-MEM (Gibco) with 10% FBS (Sigma), 0.2 mM ascorbic acid (Sigma), 100 U/mL penicillin, and 100 mg/mL streptomycin (Gibco) for proliferation. To study osteogenesis and mineralization of cells, hMSCs were then cultured in osteogenic medium, which consists of a basic medium plus 10 nM dexamethasone and 0.01 M b-glycerol phosphate. HUVECs were ordered from Lonza and then cultured in endothelial growth medium (EGM-2; Lonza). Cells at passages 3–6 were used for all the experiments. The culture medium was refreshed after 48 h. Monocultures and cocultures of cells were treated with different media in 2D well plate, as explained in Supplementary Table S1. Optical microscopic images of both cocultures and monocultures in mix medium showed normal cell morphology and clear cell proliferation after 7 days (Supplementary Fig. S1). Only HUVECs cultured with osteogenic medium were dead after 7 days. Therefore, mix medium was applied for coculture studies.

Optimization of cell ratio

The optimization studies of cell ratios were carried out on random fibrous scaffolds. The diameter of each electrospun sample for cell culture was 15 mm. hMSCs and HUVECs were trypsinized separately, and then cocultured on electrospun scaffolds. The influence of cell ratio on hMSCs osteogenic differentiation was tested using the following groups: 98:2 (hMSCs:HUVECs), 90:10, 70:30, and 50:50. Monocultures of hMSCs and HUVECs were also performed as controls. Both monocultures and cocultures of cells were seeded on scaffolds at the same total density of 2×10^4 cells/cm^2.

Cell morphology and orientation

After 7 days culture, cocultured cells were stained with F-actin and nuclei to quantitatively analyze the morphology of cells on random and aligned scaffolds. Cell scaffolds were fixed with 4% w/v formaldehyde for 30 min at room temperature. After the permeabilization with 0.1% v/v Triton X-100, cells were stained for F-actin using Alexa Fluor 488 phalloidin diluted in PBS (1:200; Fisher Scientific) for 1 h. For nuclei staining, cells were stained using DAPI diluted PBS solution (1:200; Sigma-Aldrich) for 5 min. Finally, images were taken by a fluorescence microscope (Nikon Eclipse Ti-S). Nuclear and cellular orientation was analyzed using CellProfiler 3.1.5. The cells cultured on electrospun scaffolds after 7 days were also observed by SEM. After fixation, the samples were dehydrated for 15 min at different gradient concentrations of ethanol (30%, 50%, 70%, 80%, 90%, 96%, and 100%). Cell scaffolds were then immersed with hexamethyldisilazane (HMDS; Sigma-Aldrich) for 15 min twice and dried in flow hood overnight. Dehydrated samples were gold sputtered and imaged under the SEM.

Live/dead assay and Dil-acetylated low-density lipoprotein staining

The cytotoxicity of hMSCs/HUVECs cocultured on the scaffolds was examined by live/dead staining (Fisher Scientific). Cells were rinsed with warm PBS after 1 day of culture, then stained for 30 min with 200 μL of 1 μM Calcein-AM and 6 μM ethidium homodimer-1 (EthD-1) diluted in PBS. The samples were washed with 200 μL PBS for three times before imaging. Uptake of Dil-acetylated low-density lipoprotein (Dil-Ac-LDL) was applied to identify HUVECs in our coculture system. Cell scaffolds were incubated with 200 μL Dil-Ac-LDL (10 μg/mL; Bioquote) in mix medium for 4 h. After incubation, scaffolds were rinsed in PBS for three times before imaging under the fluorescence microscope (Nikon Eclipse Ti-S).

Cell viability

Cell viability was measured at days 7 and 21 using the PrestoBlue™ reagent (Fisher Scientific). After washing with PBS, cell scaffolds were put in incubator for 30 min with culture medium supplemented with PrestoBlue reagent diluted 1:9. One hundred microliters of solution were transferred to a black 96-well plate with clear bottom and fluorescence was measured on a microplate reader (CLARIOstar; BMG Labtech) at 590 nm.

Quantification of DNA

The proliferation of cells on the random and aligned nanofibrous scaffolds was quantified by the CyQUANT™ Cell Proliferation Assay (Fisher Scientific). In brief, cell-seeded

scaffolds were washed with PBS for three times, and lysated with Tris/EDTA solution containing Proteinase K overnight at 56°C. Then, following the manufacturer's manual, RNAse buffer and Gr-dye solution were added. The fluorescence of the solution was measured on the microplate reader with excitation at 480 nm and emission detection at 520 nm.

ALP activity

Cells were incubated after 14 days in mix medium, and ALP activity was quantified by using a CDP-Star kit from Roche. Cell lysates were obtained by the treatment with cell lysis buffer (0.1 M KH_2PO_4, 0.1 M K_2HPO_4, and 0.1% Triton X-100) for 1 h, and then immersed with CDP-Star reagent for 15 min. The absorbance was detected at 466 nm by a microplate reader, then results were normalized to DNA content.

Immunostaining

Cells were washed twice in PBS and then fixed by 4% w/v formaldehyde for 30 min. After fixation, the cells were permeabilized with 0.1% Triton X-100 for 15 min and followed by blocking with block buffer, which include 1% bovine serum albumin (BSA; VWR), 0.05% Tween20 (VWR), and 5% goat serum (Sigma-Aldrich) in PBS. The primary antibodies used to target interested proteins were VE-cadherin and osteopontin (OPN) (1:200 dilute in block buffer). Secondary antibodies (including Goat anti-Mouse Alexa Fluor 488 and Goat anti-Rabbit Alexa Fluor 568) were 1:200 diluted with 0.05% Tween20 and 1% BSA in PBS. After incubating with primary antibodies overnight, secondary antibodies were added to scaffolds and soaked for 1 h. The samples were then washed with PBS for three times. Fluorescence images were captured by a fluorescence microscope (Nikon Eclipse Ti-S).

Alizarin red S staining

To observe the calcium deposits produced by cells differentiated into osteoblasts, Alizarin red S staining was performed at day 28. After fixation steps as mentioned above, scaffolds were rinsed twice in distilled water and incubated with 2% Alizarin Red S (VWR) solution (pH = 4.2) at room temperature for 2 min. Scaffolds were rinsed in distilled water for five times to wash off the excess dye. For quantitative analysis of Alizarin red S staining, stained samples were transferred into a microcentrifuge tube and dissolved in 30% acetic acid solution. After heating at 85°C for 10 min, samples were put on ice for 5 min until fully cooled. Sample solutions were centrifuged for 15 min at 20,000 rcf, and the supernatant was collected to a new microtube. About 30% ammonium hydroxide was added into tube to neutralize the pH between 4.1 and 4.5. Finally, sample solution was transferred into a 96-well plate with transparent bottom and measured by a microplate spectrophotometer (CLARIOstar; BMG Labtech) at 405 nm.

Statistical analysis

All data were shown as mean ± standard deviation. Statistical analysis was performed by using GraphPad Prism 8. One-way ANOVA with Tukey's multiple comparisons test was carried out to assess statistical differences between different groups. In all cases, significance was shown as $*p < 0.05$, $**p < 0.01$, $***p < 0.001$, and $****p < 0.0001$.

Results and Discussion

Morphology and coherency of different PCL-aligned fibers

Figure 2 shows the SEM images of different aligned electrospun PCL fibers, along with their coherency distribution and fiber diameter. As it can be seen from Figure 2a–d, by increasing the rotating speed of the collecting mandrel, more oriented and aligned fibers can be obtained. The level of alignment was also proved by the coherency coefficients (Fig. 2e). The value of coherency was close to 1 representing a highly coherent orientation and greater alignment.[52] It can be observed that the high-speed rotation of the mandrel led to a high coherency value of the fibers, hence to

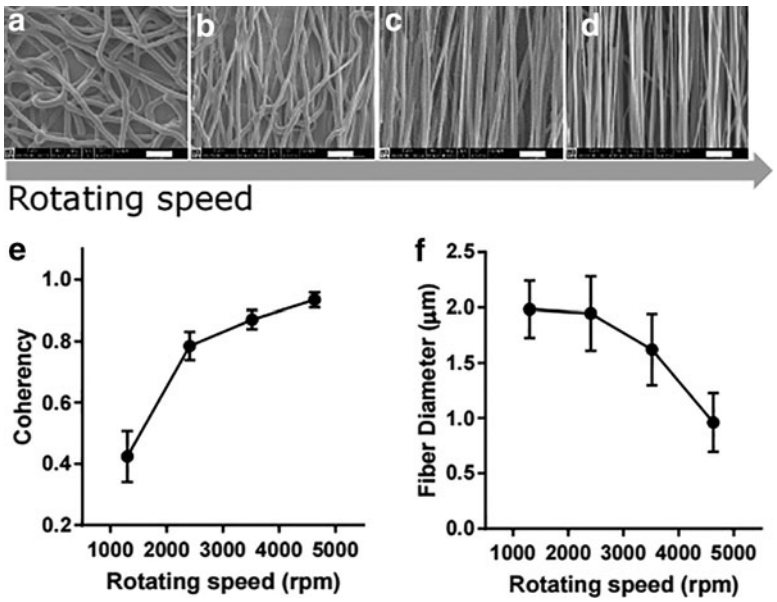

FIG. 2. SEM images **(a–d)** showing the morphology of aligned electrospun fibers produced from different rotating speed of mandrel (scale bar: 10 µm). **(e)** The effects of rotating speed on the coherency of the aligned PCL elecrospun fibers. **(f)** The diameter of different aligned PCL electrospun fibers. PCL, poly(caprolactone); SEM, scanning electron microscopy.

a high alignment of the fibers. Moreover, as the rotating speed increased to 4600 rpm, a decreasing trend for the diameter of PCL-aligned fibers was observed (Fig. 2f). We found that the rotating speed of the mandrel was negatively correlated with fiber diameter. In the production of aligned nanofibers using different rotating speed, the polymer solution was continuously extruded from the tip of the needle while stretching the polymer fibers toward the rotating collector. A higher rotating speed of the mandrel led to enhanced stretch of the fibers toward the mandrel, which gave higher fiber alignment and smaller fibers. This result was consistent with previous studies.[41,53–55] A rotating speed of 4600 rpm was found to be the best condition for the production of aligned nanofibers in our study.

Characterization of electrospun PCL random and aligned fibers

Random PCL fibrous scaffolds were fabricated by electrospinning a PCL solution onto a flat collector, while the aligned fibrous scaffolds were collected on a high rotating speed of the mandrel. SEM images showed a significant difference in the surface morphology of PCL random and aligned fibrous scaffolds (Fig. 3a, b). The majority of the fibers in the random scaffolds had an irregular arrangement and generated an fast Fourier transform output image containing pixels distributed in a symmetrical, circular shape. In contrast, the aligned fibrous scaffold generated an output image containing pixels distributed in a nonrandom, elliptical distribution. This distribution occurred because the pixel intensities were preferentially distributed with a specific orientation in aligned SEM images, whereas the frequency at which specific pixel intensities occurred in the random SEM image was theoretically identical in any direction.[56] Analysis of the SEM images showed that the coherency factor of aligned PCL fibers was statistically higher ($p < 0.0001$) than that of the randomly oriented PCL fibers (Fig. 3c). Both random and aligned fibrous scaffolds showed uniform fibers with similar fiber diameters of 1.11 ± 0.22 and $0.96 \pm 0.27\,\mu m$ (Fig. 3d).

Optimization of cell ratio

Coculture of MSCs and ECs was considered to be an excellent prevascularization approach for bone regeneration. To find out the best combinations of coculture, HUVECs and hMSCs were cocultured at different ratios (98:2–50:50) on random electrospun scaffolds. hMSCs osteogenic differentiation with different cell ratios was evaluated by measuring ALP activity. As it is shown in Figure 4a, significantly higher ALP activity was found in 90:10 coculture on day 14 compared with 98:2, 70:30, 50:50, hMSC, and HUVEC monocultures ($p < 0.001$). For both 90:10 and 98:2 groups, the ALP activity was higher than hMSCs monoculture. Results indicated that the presence of lower amount of HUVECs significantly promoted osteogenic differentiation of hMSCs. Previous reports also observed higher ALP activity when hMSCs were cocultured with a lower ratio of HUVECs.[15,49] These studies suggested that the crosstalk between the hMSCs and HUVECs might be able to secrete cytokines, such as bone morphogenetic proteins (BMPs), which could enhance the osteogenesis of hMSCs.[57] Our results correlated well with those of previous reports, revealing that coculture ratios had a significant effect on the ALP activity and especially a lower ratio of HUVECs to hMSCs was considered to benefit osteogenic differentiation.

Calcium deposition is commonly used as a late marker for osteogenic differentiation.[44] Alizarin red S staining was used to visualize and quantify the total volume of mineralization. Representative Alizarin red S staining images after 4 weeks of cell culture are shown in Figure 4c. The staining images showed that the mineralization in hMSCs

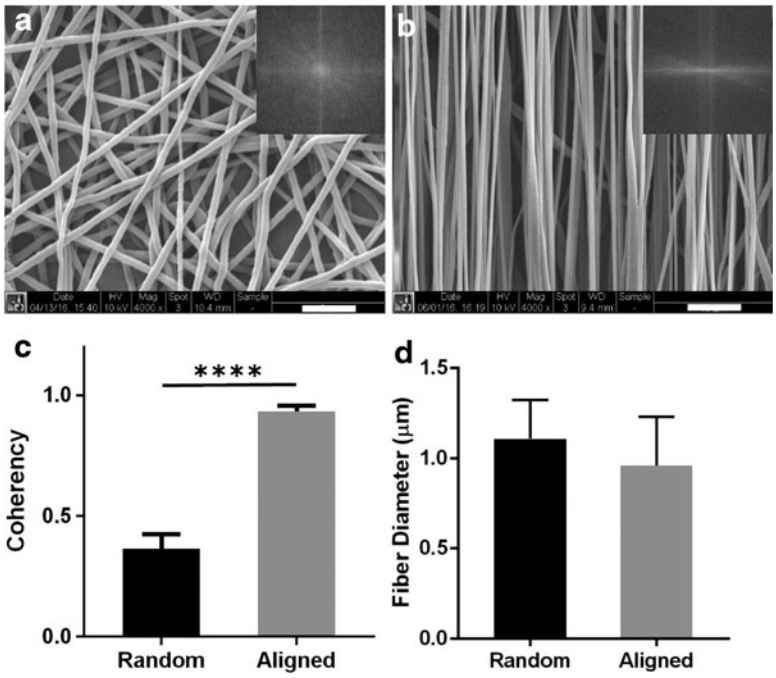

FIG. 3. SEM images **(a, b)**, alignment coherence **(c),** and average diameters **(d)** of random and aligned PCL electrospun fibers (scale bar: 10 μm). *Inset* in SEM images **(a, b)** are FFT output images of random and aligned fibers (****$p < 0.0001$). FFT, fast Fourier transform.

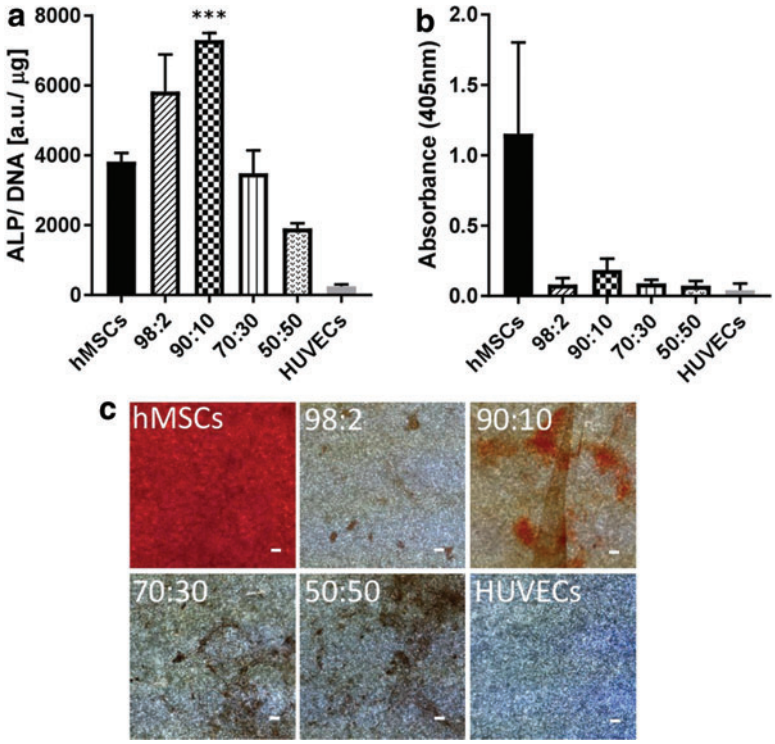

FIG. 4. **(a)** ALP activity expression in hMSCs and HUVECs on the PCL random scaffolds in monocultures and cocultures after 14 days of incubation. **(b)** Quantification of the degree of mineralization as measured by Alizarin red S staining. Representative images **(c)** of Alizarin red S staining cells cultured on the random electrospun sacffolds in mono- and coculture systems for 4 weeks (scale bar: 100 μm) (***$p < 0.001$). ALP, alkaline phosphate; HUVECs, human umbilical vein endothelial cells. Color images are available online.

monoculture was much higher than that in other groups, since this group was set as positive control and only cultured in osteogenic medium. The ratio of 90:10 coculture was the one resulting in the higher Alizarin red S staining compared with other coculture groups. These results were also supported by staining intensity quantification (Fig. 4b). Based on the present results of ALP activity and Alizarin red S staining, a 90:10 ratio of hMSCs/HUVECs cocultured on random scaffolds is regarded as the optimal ratio for osteogenic differentiation *in vitro*.

Live/dead staining and Dil-Ac-LDL uptake in hMSCs/HUVECs coculture

Live/dead staining was used to assess cytotoxicity of hMSCs/HUVECs cocultured on PCL fibrous scaffolds after 24 h seeding. Figure 5a and b shows representative images of live/dead assay staining on random and aligned electrospun scaffolds. Green color indicates the viable cells, while dead cells are red. Most of the cells were stained green, very few red cells were found in the images. It means that the majority of the cells were alive on both scaffolds after 24 h culture. Both hMSCs and HUVECs cultured on scaffolds were attached and grew well. The live ratios on random and aligned scaffolds were determined to be 92% ± 4% and 93% ± 2%, respectively. Live/dead assay showed that there was no cytotoxicity of hMSCs and HUVECs on PCL random and aligned scaffolds in our system. PCL fibrous scaffolds offered good support for hMSCs and HUVECs growth.

To prove that the system contained ECs in the coculture system, Dil-Ac-LDL was used to only stain HUVECs after culturing for 1 day. Both hMSCs and HUVECs showed DAPI staining (Fig. 5c, d), whereas the red fluorescence of Dil-Ac-LDL was only detected in HUVECs. The red staining clearly shown in the images indicated that the constructs contained HUVECs on cell-seeded random and aligned scaffolds.

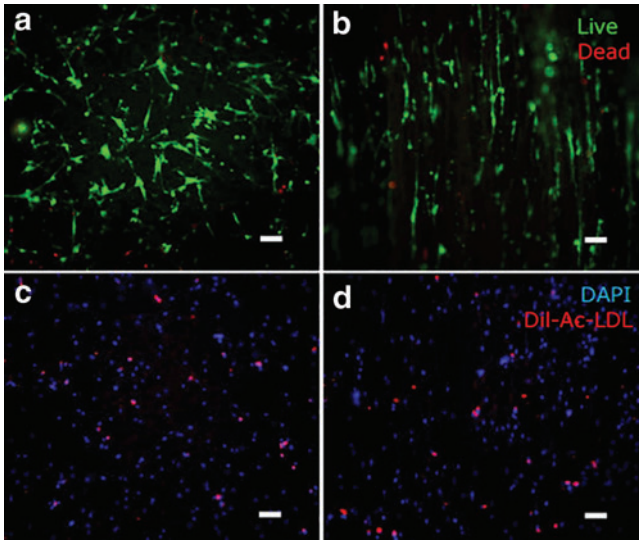

FIG. 5. Live (stained green) and dead (stained red) staining of hMSCs–HUVECs coculture system cultured for 1 day on random **(a)** and aligned **(b)** electrospun PCL fibers. hMSCs–HUVECs cultured on random **(c)** and aligned **(d)** PCL fibrous scaffolds after day 1 were stained by Dil-ac-LDL (*red*) and DAPI (*blue*). Only HUVECs showed positive for Dil-ac-LDL staining (scale bar: 100 μm). Dil-ac-LDL, Dil-acetylated low-density lipoprotein. Color images are available online.

Cell morphology and orientation on random and aligned scaffolds

Significant differences were observed in cell spreading and morphology among different scaffolds after 7 days of culture (Fig. 6a, b). Generally, the cells on the random scaffolds had disorganized actin filaments without particular orientation, while cells on the aligned scaffolds showed a large number of actin filaments parallel to the orientation of PCL fibers and exhibited a polarized morphology. Both the nuclei and cell bodies were significantly more elongated when cultured on aligned scaffolds compared with those on random scaffolds. The nuclear and cellular orientation degree of cells was measured to quantify cell alignment (Fig. 6c, d). The distribution of nuclear and cellular orientation had a similar trend. In the aligned scaffolds, ~80% of the cells had an orientation between 65° and 90°, which suggests that cells seeded on aligned scaffolds were

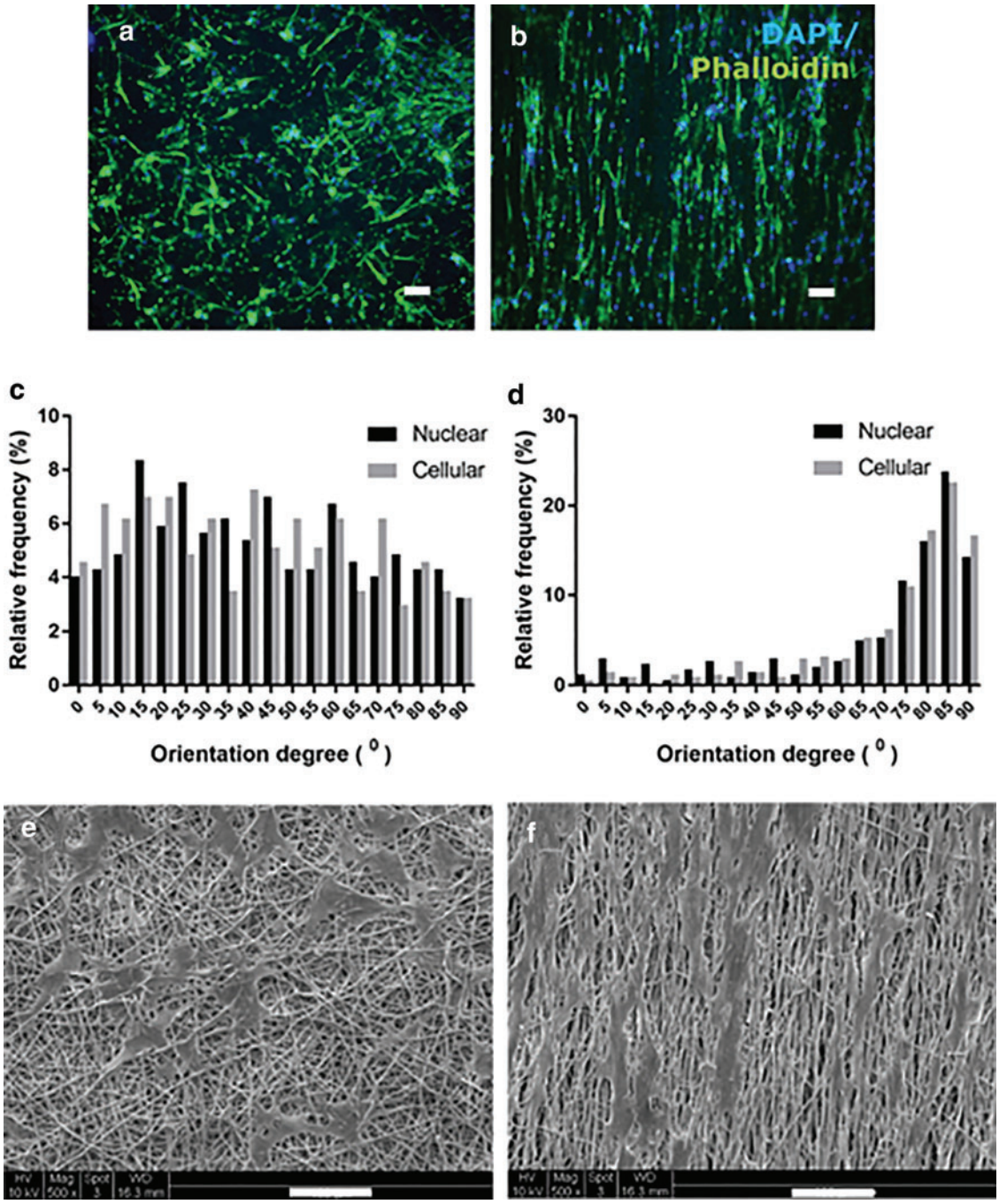

FIG. 6. Fluorescence images stained for F-actin (phalloidin: *green*) and nuclei (DAPI: *blue*) of hMSCs–HUVECs on random **(a)** and aligned **(b)** PCL electrospun scaffolds after 7 days of coculture (scale bar: 100 μm). The nuclear and cellular orientation degree of cells cultured on random **(c)** and aligned **(d)** electrospun fibers. SEM images of hMSCs–HUVECs on random **(e)** and aligned **(f)** PCL fibers after 7 days culture (scale bar: 100 μm). Color images are available online.

elongated and stretched along the preferred fiber direction. On the random scaffolds, a random distribution of cell orientation from 1° to 90° was presented. The SEM images were consistent with the immunostaining observations (Fig. 6e, f).

Prestoblue and DNA assay

The metabolic activity of cells after coculturing 7 and 21 days was assessed with Prestoblue assay. As observed in Figure 7a, the metabolic activity rate of hMSCs/HUVECs cocultured on random fibers was similar to that on aligned fibers ($p > 0.05$). Cells cocultured on both fibrous scaffolds after day 21 showed statistically significant increase of the metabolic activity compared with cells cultured for 7 days ($p < 0.0001$). The increase in metabolic activity rate after 21 days could be ascribed to cell proliferation. The DNA quantification of hMSCs/HUVECs coculture indicated a similar trend to the metabolic activity assay, which presented a significant increase of proliferation at day 21 compared with day 7 (Fig. 7b). The DNA content on random scaffolds changed from 0.1 ± 0.01 to 0.35 ± 0.11 μg/mL after 7 and 21 days culture, while that of aligned scaffolds increased from 0.20 ± 0.06 to 0.43 ± 0.03 μg/mL. DNA results indicated that both random and aligned scaffolds could support cell proliferation. However, there were still no statistical differences in DNA content between random and aligned groups ($p > 0.05$). It can be concluded that the cell proliferation on random and aligned scaffolds may not be significantly different. This result is consistent with previous results, reporting that the fiber orientation did not alter cell proliferation.[38]

ALP activity

ALP activity was used to examine the early osteogenic differentiation of hMSCs. The ALP activity of different cells on fibrous scaffolds at day 14 was measured and shown in Figure 7c. For both random and aligned scaffolds, the ALP activity was significantly higher in coculture than that in monoculture ($p < 0.01$), indicating that HUVECs supported osteogenesis of hMSCs. We also compared the ALP activity between cells cultured on random and aligned scaffolds. However, there were no statistical differences between hMSCs cultured on different scaffolds ($p > 0.05$). Our study demonstrated that fiber alignment did not have much effect on ALP activity of hMSCs. A similar trend was also found in the coculture group. These results clearly indicated that fiber alignment did not play an important role in hMSCs osteogenic differentiation, while coculture with HUVECs actively induced early osteogenic differentiation of hMSCs.

Previous studies studying whether random and aligned topography of nanofibers affects MSCs osteogenic differentiation are controversial. Wang *et al.* showed that fiber alignment enhanced osteogenic differentiation: for example, MSCs cultured on the aligned PHBHHx microfibers showed relatively high expression of osteogenic genes, including osteocalcin, runx2, OPN, and osteonectin, compared with that on random fiber.[58] Yin *et al.* however demonstrated that MSCs grew on randomly poly(L-lactic acid) (PLLA) fibrous scaffolds presented enhanced ALP staining and osteogenic marker genes (osteocalcin and runx2) compared with cells on aligned PLLA fibrous scaffolds.[59] Few studies also reported that fiber alignment guided the orientation of adherent cells, but did not influence osteogenic differentiation.[38,41] In the presence of HUVECs, our results are consistent with observations where the aligned fibers provide oriented tissue but do not significantly influence osteogenic differentiation.[38,41]

Immunostaining

After 21 days, the formation of vascularized bone tissue on different scaffolds was evaluated by the immunofluorescence staining of an osteogenic differentiation marker OPN (shown in red) and an angiogenic specific marker (VE-cadherin, shown in green), respectively. OPN is a key marker of osteogenesis and biomineralization.[60] Immunostaining for OPN showed a robust expression in cells cultured on random and aligned scaffolds (Fig. 8a, b).

Moreover, immunofluorescent staining for VE-cadherin (Fig. 8c, d) revealed the formation of an interconnected

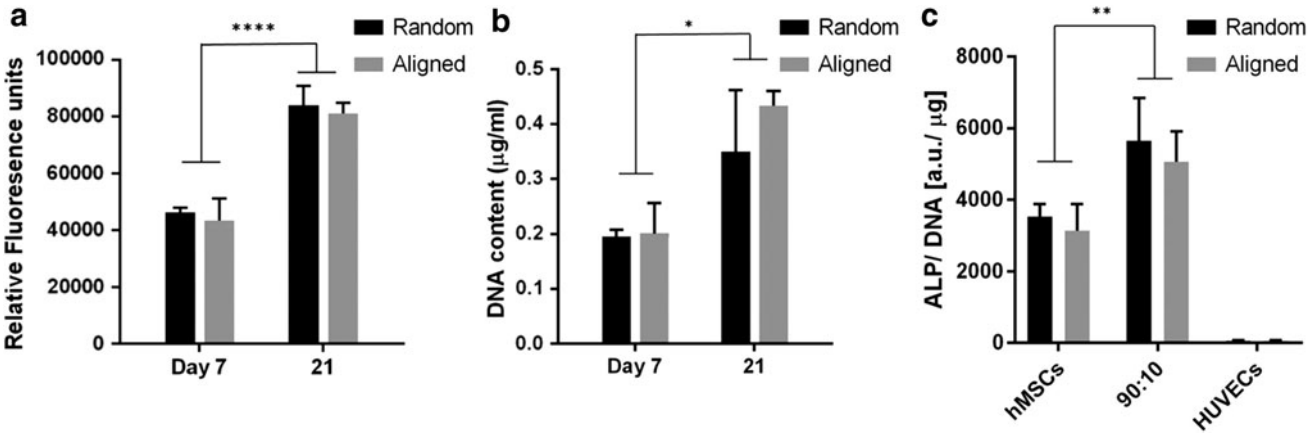

FIG. 7. Metabolic activity **(a)** and proliferation **(b)** of hMSCs–HUVECs cultured for 7 and 21 days on PCL electrospun fibers. **(c)** ALP activity expression in hMSCs–HUVECs on the PCL random and aligned scaffolds after 14 days of culture (*$p < 0.05$, **$p < 0.01$, and ****$p < 0.0001$).

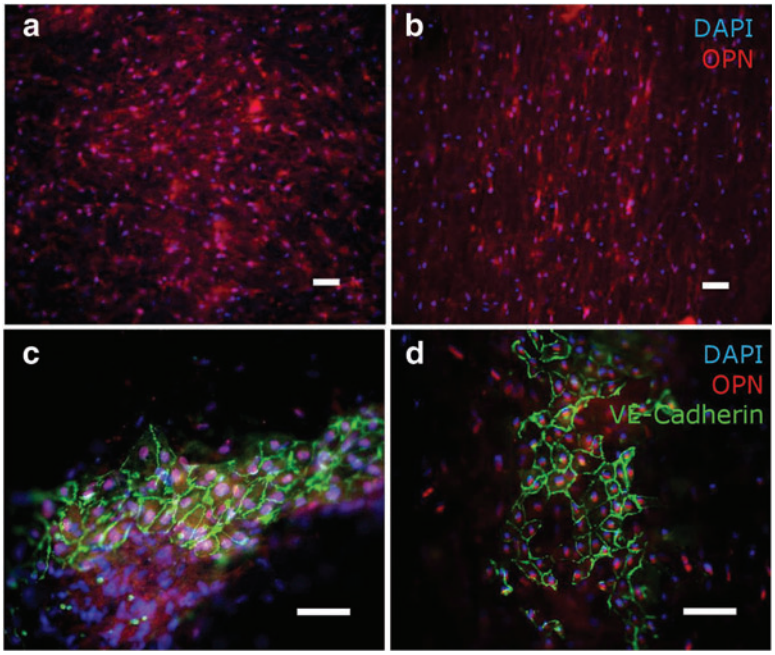

FIG. 8. OPN (osteogenesis marker; *red*) immunostaining of hMSCs cultured on the random **(a)** and aligned **(b)** PCL electrospun fibers in coculture with HUVECs for 21 days. Graphs **(c, d)** showing expression of endothelial marker, VE-cadherin (*green*), by HUVECs in coculture with hMSCs at day 21 on random and aligned scaffolds (scale bar: 100 μm). OPN, osteopontin. Color images are available online.

EC layer in coculture conditions. The localization of these proteins at the cell–cell borders is consistent with their functions as ECs adhesion molecules.[61] Both random and aligned scaffolds showed the expression of VE-cadherin at EC junctions in hMSCs–HUVECs coculture. Nuclear staining with DAPI was used to detect all cells, including hMSCs, which did not express VE-cadherin. The localization of hMSCs was adjacent to the endothelial network formed by HUVECs, suggesting that hMSCs could be acting as pericytes to stabilize the networks.[61–63] Our study did not show robust vascular network formation due to the low amount of HUVECs in coculture. However, cells on both scaffolds showed relative expression of VE-cadherin. Taken together, these results indicate that a 90:10 coculture ratio of hMSCs and HUVECs on both random and aligned scaffolds exhibited enhanced osteogenesis and the ability of generating intercellular junctions.

Alizarin Red S staining

The osteogenic differentiation of hMSCs on the scaffolds was further analyzed through staining calcium deposits with Alizarin red (Fig. 9). This mineralization assay demonstrated positive Alizarin red staining from hMSCs monoculture and coculture group in comparison with HUVECs monoculture. Significant higher staining of calcium deposits was shown in hMSCs/HUVECs coculture than hMSCs monoculture ($p < 0.05$). These results are consistent with other literature, which demonstrated that 90:10 cocultures of hMSCs with ECs increased osteogenic differentiation.[47] However, no significant difference was found between hMSCs monoculture and coculture on random and aligned fibrous scaffolds ($p > 0.05$). Hence, fiber alignment did not influence hMSCs mineralization. This finding suggests that the coculture with ECs strongly promoted the osteogenesis of hMSCs, while fiber alignment did not.

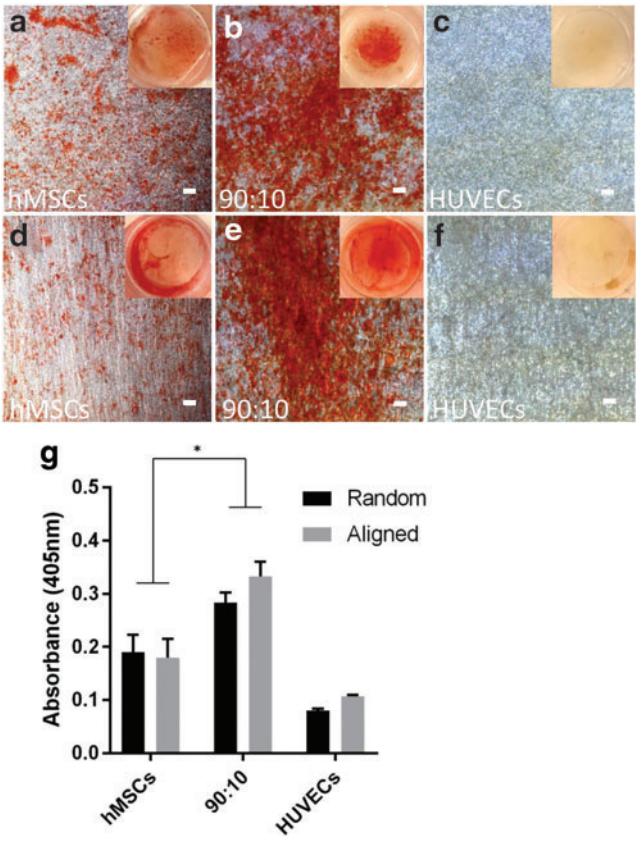

FIG. 9. **(a-f)** Representative images of Alizarin red S staining cells cultured on the random and aligned electrospun sacffolds in mono- and coculture systems for 4 weeks (scale bar: 100 μm). **(g)** Quantification of the degree of mineralization as measured by Alizarin red S staining ($*p < 0.05$). Color images are available online.

Conclusion

In summary, we fabricated random and aligned PCL fibrous scaffolds to evaluate the combinatorial influence of fiber orientation and coculture with ECs on hMSCs osteogenic differentiation. The optimization of coculture results indicated that the 90:10 of hMSCs/HUVECs cultured on random and aligned fibrous scaffolds appeared to be the optimal ratio for osteogenesis of hMSCs. Fiber alignment strongly influenced cell morphology and orientation, but did not show an important impact on hMSCs osteogenic differentiation. Moreover, the addition of ECs to hMSCs enhanced their osteogenic differentiation, as shown by ALP activity and mineralization of hMSCs. The intercellular junctions organized by ECs were apparent when cocultured with hMSCs on scaffolds. These results indicated that cocultures with ECs have more influence on bone regeneration than fiber alignment; in addition, structural properties of scaffolds (such as fiber alignment) can control orientation and distribution of cells, which may be used to engineer bone tissue with defined direction.

Disclosure Statement

No competing financial interests exist.

Funding Information

We are supported by China Scholarship Council (Grant No. 201508610081). This research project has been made possible thanks to the support of the Dutch Province of Limburg.

Supplementary Material

Supplementary Table S1
Supplementary Figure S1

References

1. Kang, Y., Kim, S., Fahrenholtz, M., Khademhosseini, A., and Yang, Y. Osteogenic and angiogenic potentials of monocultured and co-cultured human-bone-marrow-derived mesenchymal stem cells and human-umbilical-vein endothelial cells on three-dimensional porous beta-tricalcium phosphate scaffold. Acta Biomater **9,** 4906, 2013.
2. Grellier, M., Bordenave, L., and Amedee, J. Cell-to-cell communication between osteogenic and endothelial lineages: implications for tissue engineering. Trends Biotechnol **27,** 562, 2009.
3. Stegen, S., van Gastel, N., and Carmeliet, G. Bringing new life to damaged bone: the importance of angiogenesis in bone repair and regeneration. Bone **70,** 19, 2015.
4. Yu, H., VandeVord, P.J., Mao, L., Matthew, H.W., Wooley, P.H., and Yang, S.-Y. Improved tissue-engineered bone regeneration by endothelial cell mediated vascularization. Biomaterials **30,** 508, 2009.
5. García, J.R., and García, A.J. Biomaterial-mediated strategies targeting vascularization for bone repair. Drug Deliv Transl Res **6,** 77, 2016.
6. He, X., Dziak, R., Yuan, X., *et al*. BMP2 genetically engineered MSCs and EPCs promote vascularized bone regeneration in rat critical-sized calvarial bone defects. PLoS One **8,** e60473, 2013.
7. Logeart-Avramoglou, D., Anagnostou, F., Bizios, R., and Petite, H. Engineering bone: challenges and obstacles. J Cell Mol Med **9,** 72, 2005.
8. Santos, M.I., and Reis, R.L. Vascularization in bone tissue engineering: physiology, current strategies, major hurdles and future challenges. Macromol Biosci **10,** 12, 2010.
9. Park, H., Lim, D.-J., Sung, M., Lee, S.-H., Na, D., and Park, H. Microengineered platforms for co-cultured mesenchymal stem cells towards vascularized bone tissue engineering. Tissue Eng Regen Med **13,** 465, 2016.
10. Stoppato, M., Stevens, H., Carletti, E., Migliaresi, C., Motta, A., and Guldberg, R. Influence of scaffold properties on the inter-relationship between human bone marrow derived stromal cells and endothelial cells in pro-osteogenic conditions. Acta Biomater **25,** 16, 2015.
11. Jin, G.-Z., Han, C.-M., and Kim, H.-W. In vitro co-culture strategies to prevascularization for bone regeneration: a brief update. Tissue Eng Regen Med **12,** 69, 2015.
12. Unger, R.E., Ghanaati, S., Orth, C., *et al*. The rapid anastomosis between prevascularized networks on silk fibroin scaffolds generated in vitro with cocultures of human microvascular endothelial and osteoblast cells and the host vasculature. Biomaterials **31,** 6959, 2010.
13. Unger, R.E., Dohle, E., and Kirkpatrick, C.J. Improving vascularization of engineered bone through the generation of pro-angiogenic effects in co-culture systems. Adv Drug Deliv Rev **94,** 116, 2015.
14. Wenger, A., Stahl, A., Weber, H., *et al*. Modulation of in vitro angiogenesis in a three-dimensional spheroidal coculture model for bone tissue engineering. Tissue Eng **10,** 1536, 2004.
15. Rouwkema, J., Boer, J.D., and Blitterswijk, C.A.V. Endothelial cells assemble into a 3-dimensional prevascular network in a bone tissue engineering construct. Tissue Eng **12,** 2685, 2006.
16. Fu, W.-L., Xiang, Z., Huang, F.-G., *et al*. Coculture of peripheral blood-derived mesenchymal stem cells and endothelial progenitor cells on strontium-doped calcium polyphosphate scaffolds to generate vascularized engineered bone. Tissue Engineering Part A 21, 948, 2014.
17. Saleh, F., Whyte, M., and Genever, P. Effects of endothelial cells on human mesenchymal stem cell activity in a three-dimensional in vitro model. Eur Cell Mater **22,** e57, 2011.
18. Mendes, L.F., Pirraco, R.P., Szymczyk, W., *et al*. Perivascular-like cells contribute to the stability of the vascular network of osteogenic tissue formed from cell sheet-based constructs. PLoS One **7,** e41051, 2012.
19. Brunette, D. The effects of implant surface topography on the behavior of cells. Int J Oral Maxillofac Implants **3,** 231, 1988.
20. Brunette, D., and Chehroudi, B. The effects of the surface topography of micromachined titanium substrata on cell behavior in vitro and in vivo. J Biomech Eng **121,** 49, 1999.
21. Flemming, R., Murphy, C.J., Abrams, G., Goodman, S., and Nealey, P. Effects of synthetic micro-and nano-structured surfaces on cell behavior. Biomaterials **20,** 573, 1999.
22. Abagnale, G., Sechi, A., Steger, M., *et al*. Surface topography guides morphology and spatial patterning of induced pluripotent stem cell colonies. Stem Cell Rep **9,** 654, 2017.
23. Dalby, M.J., Gadegaard, N., Tare, R., *et al*. The control of human mesenchymal cell differentiation using nanoscale symmetry and disorder. Nat Mater **6,** 997, 2007.

24. Engler, A.J., Sen, S., Sweeney, H.L., Discher, D.E. Matrix elasticity directs stem cell lineage specification. Cell **126,** 677, 2006.
25. Ozdemir, T., Higgins, A.M., and Brown, J.L. Osteoinductive biomaterial geometries for bone regenerative engineering. Curr Pharm Des **19,** 3446, 2013.
26. Li, H., Wen, F., Chen, H., *et al*. Micropatterning extracellular matrix proteins on electrospun fibrous substrate promote human mesenchymal stem cell differentiation toward neurogenic lineage. ACS Appl Mater Interfaces **8,** 563, 2015.
27. Rajnicek, A., Britland, S., and McCaig, C. Contact guidance of CNS neurites on grooved quartz: influence of groove dimensions, neuronal age and cell type. J Cell Sci **110,** 2905, 1997.
28. Kafi, M.A., El-Said, W.A., Kim, T.-H., and Choi, J.-W. Cell adhesion, spreading, and proliferation on surface functionalized with RGD nanopillar arrays. Biomaterials **33,** 731, 2012.
29. Park, K.S., Cha, K.J., Han, I.B., *et al*. Mass-producible nano-featured polystyrene surfaces for regulating the differentiation of human adipose-derived stem cells. Macromol Biosci **12,** 1480, 2012.
30. McMurray, R.J., Gadegaard, N., Tsimbouri, P.M., *et al*. Nanoscale surfaces for the long-term maintenance of mesenchymal stem cell phenotype and multipotency. Nat Mater **10,** 637, 2011.
31. Guo, Z., Xu, J., Ding, S., Li, H., Zhou, C., and Li, L. In vitro evaluation of random and aligned polycaprolactone/gelatin fibers via electrospinning for bone tissue engineering. J Biomater Sci Polym Ed **26,** 989, 2015.
32. Jahani, H., Kaviani, S., Hassanpour-Ezatti, M., Soleimani, M., Kaviani, Z., and Zonoubi, Z. The effect of aligned and random electrospun fibrous scaffolds on rat mesenchymal stem cell proliferation. Cell J **14,** 31, 2012.
33. Fantner, G.E., Birkedal, H., Kindt, J.H., *et al*. Influence of the degradation of the organic matrix on the microscopic fracture behavior of trabecular bone. Bone **35,** 1013, 2004.
34. Ramasamy, J., and Akkus, O. Local variations in the micromechanical properties of mouse femur: the involvement of collagen fiber orientation and mineralization. J Biomech **40,** 910, 2007.
35. Summitt, M.C., and Reisinger, K.D. Characterization of the mechanical properties of demineralized bone. J Biomed Mater Res A **67,** 742, 2003.
36. Kim, H.N., Jiao, A., Hwang, N.S., Kim, M.S., Kim, D.-H., and Suh, K.-Y. Nanotopography-guided tissue engineering and regenerative medicine. Adv Drug Deliv Rev **65,** 536, 2013.
37. Xie, J., Li, X., Lipner, J., *et al*. ''Aligned-to-random'' nanofiber scaffolds for mimicking the structure of the tendon-to-bone insertion site. Nanoscale **2,** 923, 2010.
38. Ma, J., He, X., and Jabbari, E. Osteogenic differentiation of marrow stromal cells on random and aligned electrospun poly (L-lactide) nanofibers. Ann Biomed Eng **39,** 14, 2011.
39. Xu, Y., Wu, Z., Dong, X., and Li, H. Combined biomaterial signals stimulate communications between bone marrow stromal cell and endothelial cell. RSC Adv **7,** 5306, 2017.
40. Kolambkar, Y.M., Bajin, M., Wojtowicz, A., Hutmacher, D.W., García, A.J., and Guldberg, R.E. Nanofiber orientation and surface functionalization modulate human mesenchymal stem cell behavior in vitro. Tissue Eng Part A **20,** 398, 2013.
41. Madhurakkat Perikamana, S.K., Lee, J., Ahmad, T., *et al*. Effects of immobilized BMP-2 and nanofiber morphology on in vitro osteogenic differentiation of hMSCs and in vivo collagen assembly of regenerated bone. ACS Appl Mater interfaces **7,** 8798, 2015.
42. Naito, Y., Shinoka, T., Duncan, D., *et al*. Vascular tissue engineering: towards the next generation vascular grafts. Adv Drug Deliv Rev **63,** 312, 2011.
43. Liu, Y., Chan, J.K., and Teoh, S.H. Review of vascularised bone tissue-engineering strategies with a focus on co-culture systems. J Tissue Eng Regen Med **9,** 85, 2015.
44. Ma, J., van den Beucken, J.J., Yang, F., *et al*. Coculture of osteoblasts and endothelial cells: optimization of culture medium and cell ratio. Tissue Eng Part C Methods **17,** 349, 2010.
45. Zhou, J., Lin, H., Fang, T., *et al*. The repair of large segmental bone defects in the rabbit with vascularized tissue engineered bone. Biomaterials **31,** 1171, 2010.
46. Henrich, D., Seebach, C., Kaehling, C., *et al.* Simultaneous cultivation of human endothelial-like differentiated precursor cells and human marrow stromal cells on β-tricalcium phosphate. Tissue Eng Part C Methods **15,** 551, 2009.
47. Kazemzadeh-Narbat, M., Rouwkema, J., *et al*. Engineering photocrosslinkable bicomponent hydrogel constructs for creating 3D vascularized bone. Adv Healthc Mater **6,** 1601122, 2017.
48. Mishra, R., Roux, B.M., Posukonis, M., *et al*. Effect of prevascularization on in vivo vascularization of poly (propylene fumarate)/fibrin scaffolds. Biomaterials **77,** 255, 2016.
49. Sasaki, J.-I., Hashimoto, M., Yamaguchi, S., *et al*. Fabrication of biomimetic bone tissue using mesenchymal stem cell-derived three-dimensional constructs incorporating endothelial cells. PLoS One **10,** e0129266, 2015.
50. Yao, T., Chen, H., Samal, P., *et al*. Self-assembly of electrospun nanofibers into gradient honeycomb structures. Mater Des **168,** 107614, 2019.
51. Both, S.K., van der Muijsenberg, A.J., van Blitterswijk, C.A., de Boer, J., and de Bruijn, J.D. A rapid and efficient method for expansion of human mesenchymal stem cells. Tissue Eng **13,** 3, 2007.
52. Kobayashi, M., Lei, N.Y., Wang, Q., Wu, B.M., and Dunn, J.C. Orthogonally oriented scaffolds with aligned fibers for engineering intestinal smooth muscle. Biomaterials **61,** 75, 2015.
53. Thomas, V., Jose, M.V., Chowdhury, S., Sullivan, J.F., Dean, D.R., and Vohra, Y.K. Mechano-morphological studies of aligned nanofibrous scaffolds of polycaprolactone fabricated by electrospinning. J Biomater Sci Polym Ed **17,** 969, 2006.
54. Haider, S., Al-Zeghayer, Y., Ali, F.A.A., *et al*. Highly aligned narrow diameter chitosan electrospun nanofibers. J Polym Res **20,** 105, 2013.
55. Zander, N., Gillan, M., and Sweetser, D. Composite fibers from recycled plastics using melt centrifugal spinning. Materials **10,** 1044, 2017.
56. Ayres, C., Bowlin, G.L., Henderson, S.C., *et al*. Modulation of anisotropy in electrospun tissue-engineering scaffolds: analysis of fiber alignment by the fast Fourier transform. Biomaterials **27,** 5524, 2006.
57. Kim, J., Kim, H.N., Lim, K.-T., *et al*. Synergistic effects of nanotopography and co-culture with endothelial cells on osteogenesis of mesenchymal stem cells. Biomaterials **34,** 7257, 2013.

58. Wang, Y., Gao, R., Wang, P.-P., *et al*. The differential effects of aligned electrospun PHBHHx fibers on adipogenic and osteogenic potential of MSCs through the regulation of PPARγ signaling. Biomaterials **33,** 485, 2012.
59. Yin, Z., Chen, X., Song, H.-X., *et al*. Electrospun scaffolds for multiple tissues regeneration in vivo through topography dependent induction of lineage specific differentiation. Biomaterials **44,** 173, 2015.
60. Li, C., Armstrong, J.P.K., Pence, I.J., *et al*. Glycosylated superparamagnetic nanoparticle gradients for osteochondral tissue engineering. Biomaterials **176,** 24, 2018.
61. Wu, X., Rabkin-Aikawa, E., Guleserian, K.J., *et al*. Tissue-engineered microvessels on three-dimensional biodegradable scaffolds using human endothelial progenitor cells. Am J Physiol Heart Circ Physiol **287,** H480, 2004.
62. Pang, Y., Tsigkou, O., Spencer, J.A., Lin, C.P., Neville, C., and Grottkau, B. Analyzing structure and function of vascularization in engineered bone tissue by video-rate intravital microscopy and 3D image processing. Tissue Eng Part C Methods **21,** 1025, 2015.
63. Takebe, T., Koike, N., Sekine, K., *et al*. Generation of Functional Human Vascular Network. Transplant Proc **44,** 1130, 2012.

Address correspondence to:
Lorenzo Moroni, PhD
Complex Tissue Regeneration Department
MERLN Institute for Technology Inspired Regenerative Medicine
Maastricht University
6229 ER Maastricht
The Netherlands

E-mail: l.moroni@maastrichtuniversity.nl

Received: August 23, 2019
Accepted: November 8, 2019
Online Publication Date: December 31, 2019